Journal of
Computational and Theoretical Nanoscience
Vol. 5, 1–7, 2008

Characteristic Times for Pressure and Electrostatic Force Driven Thin Film Drainage

David G. Crawford, Charles R. Koch, and Subir Bhattacharjee*

Department of Mechanical Engineering, 4-9 Mechanical Engineering Building, University of Alberta, Edmonton, AB, T6G 2G8, Canada

The drainage of thin liquid films confined between two electrodes was studied employing the long wave approximation of the pertinent hydrodynamic equations. A general mathematical formulation was used for the case of electric field driven drainage of the film by solving the Laplace equation in conjunction with the approximate flow equations. The drainage of small periodic segments of the film was then studied employing the model under conditions that emulate purely pressure based drainage, as well as drainage in presence of an applied electric field. The final film morphologies and the drainage times in presence of electric fields were found to be considerably different from those observed for pressure based drainage.

Keywords: Thin Liquid Films, Electrostatic Drainage, Long Wave Approximation, Finite Difference, van der Waals Interaction.

RESEARCH ARTICLE

1. INTRODUCTION

Thin macroscopic films occur in a wide range of biological, physical and engineering systems. When the films are subjected to mechanical, thermal, chemical, or electrical perturbations, their drainage can occur due to a diverse range of dynamics such as wave propagation, wave steepening, and chaotic responses. The films may or may not rupture, holes or dry spots may form, and other complicated structures may result. The phenomena that govern thin film drainage are different than those in typical bulk fluids and present unique challenges.[1] In thin films, with thickness <100 nm, fluid molecules interact not only with surrounding fluid molecules (as in a typical bulk environment) but also the materials that bound the film.[2,3] The strength and range of the intermolecular forces depend on the physical and chemical properties of the system, and are predominantly classified as the Lifshitz van der-Waals (LVDW), electrostatic, and polar interactions.[3] The excess intermolecular interactions result in a conjoining/disjoining pressure, which causes film drainage.

Modification of the drainage behavior of films by applying an electric field has immense importance in a variety of applications, including formation of well-controlled patterns leading to novel nanostructures of relevance to optoelectronic devices, sensors, biochips, and membranes.[4] Considerable theoretical attention has been devoted to elucidate pattern formation in thin polymeric films by application of electric fields.[5–9] Most of these studies primarily devote their attention to the relationship between the pertinent length scales and the range of the interactions that determine the final structure of the film after drainage. In this context, a comparison of the time scales between conventional pressure based drainage and electric field induced drainage has not been a major focus of these studies. Some of our recent experiments with electric field induced drainage of free films lead to the notion that electric fields result in a much more rapid drainage of the films, and the ensuing patterns can be more complex compared to pressure induced drainage.[10] To address this observation, this paper theoretically explores the electric field induced drainage of thin films supported by a solid substrate, and compares the drainage times and final patterns with those obtained during solely pressure based drainage.

2. MATHEMATICAL MODEL

When a thin film is perturbed by an infinitesimal disturbance, the perturbations may grow or be damped out. If the film is thicker then a critical thickness, the perturbations will grow in a periodic manner creating waves on the film surface.[2,11] The perturbations grow with a characteristic wavelength (λ). The wavelengths of the disturbance are much larger than the mean film thickness. The difference in length scale between the film thickness and the

*Author to whom correspondence should be addressed.

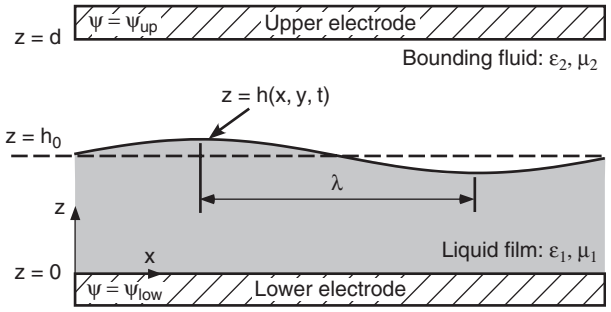

Fig. 1. Schematic representation of the thin film system. The liquid film under consideration is supported by the lower electrode. The bounding fluid is modeled as an inert fluid (similar to air) with $\mu_2 \ll \mu_1$. For electrostatic force induced drainage, a potential difference of $\psi_{low} - \psi_{up}$ is applied between the two electrodes, with ψ_{up} typically set as ground. The initial height of the unperturbed film is h_0 and the vertical distance between the two electrodes is d.

waves that form on the film interface allow the simplification of the governing equations. A 'long-wave' asymptotic analysis can be used to simplify the governing equations.[1]

The thin film system studied is shown schematically in Figure 1. It depicts a liquid film with a bounding fluid on top, sandwiched between two electrodes. As shown in the figure, d is the electrode spacing, $h(x, y, t)$ is the film thickness at spatial coordinates (x, y) and time (t), h_0 is the average initial film thickness, subscript i indicates the fluid phase under consideration with $i = 1$ for the film and $i = 2$ for the bounding fluid, ϵ_i $(i = 1, 2)$ indicates the permittivity of fluid i, μ_i is the viscosity of fluid $(i = 1, 2)$, λ is the wavelength of disturbances on the film interface, ψ_{up} is an applied voltage at upper electrode $(z = d)$ and ψ_{low} is the applied voltage at the lower electrode $(z = 0)$.

2.1. Governing Equations

The fluids are modeled using a continuum assumption and the motion is defined by the Navier Stokes (NS) equations and a continuity relation.

$$\rho_i\left(\frac{\partial \vec{u}_i}{\partial t} + (\vec{u}_i \cdot \nabla)\vec{u}_i\right) = -\nabla p_i + \nabla \cdot [\mu_i(\nabla \vec{u}_i + (\nabla \vec{u}_i)^T)] + \vec{f}_i \quad (1a)$$

$$\nabla \cdot (\rho_i \vec{u}_i) = 0 \quad (1b)$$

The term $\vec{u}_i$ is the velocity vector $(\vec{u} = [u, v, w])$, p_i is the pressure, ρ_i is the density, ∇ is the cartesian operator $\vec{\nabla} = (\partial/\partial x, \partial/\partial y, \partial/\partial z)$, and $\vec{f}_i = -\nabla(\phi_i)$ represents the body forces, where ϕ_i is the conjoining/disjoining pressure. The conjoining/disjoining pressure is an excess energy per unit volume that describes forces that exist on the film. The Navier Stokes system shown in Eq. (1) is applied for both the film and bounding fluid $(i = 1, 2)$.

The general formulation for thin film drainage is completed by the definition of boundary conditions. At the upper and lower electrodes, no penetration and no slip boundary conditions are applied.

$$\begin{aligned} \vec{u}_1 &= 0 \quad \text{at } z = 0 \\ \vec{u}_2 &= 0 \quad \text{at } z = d \end{aligned} \quad (2)$$

At the interface between the fluids, continuity of velocity and a stress balance exist. The two fluids are modeled as immiscible, so no fluid mixing or mass transfer occurs at their interface. This ensures that a sharp interface is maintained and that velocity is continuous across it.

$$\vec{u}_1 = \vec{u}_2 \quad \text{at } z = h(x, y, t) \quad (3)$$

The velocity of the fluids at the interface is related to the film thickness by a kinematic condition.[11] The kinematic condition is obtained by taking the partial derivative of the film thickness, $z = h(x, y, t)$, with respect to time. The chain rule and velocity definitions can then be used to relate the film thickness to the interfacial velocity.

$$w = \frac{\partial h}{\partial t} + u\frac{\partial h}{\partial x} + v\frac{\partial h}{\partial y} \quad \text{at } z = h(x, y, t) \quad (4)$$

The kinematic condition in Eq. (4) is used in place of the continuity of velocity (Eq. 3).

At the interface, a stress balance between the two fluids is performed by taking the normal and tangential projections of the stresses at the fluid interface.

$$\vec{n} \cdot \{\bar{\bar{\sigma}}_1 \cdot \vec{n} - \bar{\bar{\sigma}}_2 \cdot \vec{n}\} = \kappa\gamma + \vec{f}_e \cdot \vec{n} \quad (5)$$

$$\vec{t}^j \cdot [\bar{\bar{\sigma}}_1 \cdot \vec{n} - \bar{\bar{\sigma}}_2 \cdot \vec{n}] = \vec{f}_e \cdot \vec{t}^j \quad (6)$$

where $\vec{t}^j = (t_x^{(j)}, t_y^{(j)}, t_z^{(j)})$ is the jth unit tangent vector to the fluid interface where $(j = 1, 2)$, $\vec{n}$ is the unit normal vector to the fluid interface, which points from the film to the bounding fluid with components $\vec{n} = (n_x, n_y, n_z)$, κ is the mean interfacial curvature, γ is the interfacial tension, $\vec{f}_e$ is the external surface force vector and $\bar{\bar{\sigma}}_i$ is the stress tensor for the ith fluid phase $(i = 1, 2)$.

The solution of the NS equation system presented above would be difficult since the interface between the fluids is a free boundary. Fortunately, the problem scaling and physics allow the system to be reduced to a single evolution equation for the film thickness. The 'long wave' or 'small slope' scaling argument uses the fact that dominant wavelength of disturbances, λ, which dictates the length scale of the problem, is much larger than the film thickness, h.[1, 7, 11, 12] For simplicity, a scaling factor k is defined to indicate the difference in lengths and aid in the simplification of the hydrodynamic equations

$$k = \frac{h_0}{\lambda} \ll 1 \quad (7)$$

where h_0 is the initial mean film thickness. The lengths are non-dimensionalized by using the mean film thickness h_0

RESEARCH ARTICLE

for z and the fastest growing disturbance, λ, for x and y. The scaled spatial dimensions and the spatial derivatives are explicitly given by (the uppercase variables represent the scaled quantities):

$$x = \lambda X \quad y = \lambda Y \quad z = h_0 Z \tag{8a}$$

$$\frac{\partial}{\partial x} = \frac{1}{\lambda}\frac{\partial}{\partial X} \quad \frac{\partial}{\partial y} = \frac{1}{\lambda}\frac{\partial}{\partial Y} \quad \frac{\partial}{\partial z} = \frac{1}{h_0}\frac{\partial}{\partial Z} \tag{8b}$$

Equation (8) are simplified using Eq. (7) and can be used to determine the scaling required for the other problem parameters. If the fluid velocity components in the lateral directions (x, y) will have characteristic values u_0, $v_0 = O(1)$, then the non-dimensional velocities in these directions can be written as:

$$U = \frac{u}{u_0} \quad V = \frac{v}{u_0} \tag{9}$$

The continuity Eq. (1), using relations (8) and (9), becomes:

$$\frac{u_0}{\lambda}\frac{\partial U}{\partial X} + \frac{u_0}{\lambda}\frac{\partial V}{\partial Y} + \frac{\partial w}{\partial z} = 0 \tag{10}$$

which suggests a scaling of the fluid velocity in z direction as

$$W = \frac{\lambda}{u_0 h_0} w = \frac{w}{u_0 k} \tag{11}$$

The time is re-scaled to reflect the long length scales considered, defining a new slow time (T) based on the characteristic velocity (u_0) and long length scale (λ)

$$T = \frac{k u_0}{h_0} t \tag{12}$$

Following the work of Oron et al.,[1] the flow within the film is locally parallel, so that $p_x \sim \mu u_{zz}$ and $p_y \sim \mu v_{zz}$. This suggests scaling for the pressure (P) and body forces (Φ) as:

$$(P, \Phi) = \frac{k h_0}{\mu u_0}(p, \phi) \tag{13}$$

Re-writing the NS system with the scalings introduced by Eqs. (8–13) gives:

$$k\mathrm{Re}\,(U_T + UU_X + VU_Y + WU_Z) = -(P+\Phi)_X + k^2(U_{XX} + U_{YY}) + U_{ZZ} \tag{14a}$$

$$k\mathrm{Re}\,(V_T + UV_X + VV_Y + WV_Z) = -(P+\Phi)_Y + k^2(V_{XX} + V_{YY}) + V_{ZZ} \tag{14b}$$

$$k^3\mathrm{Re}\,(W_T + UW_X + VW_Y + WW_Z) = -(P+\Phi)_Z + k^2[k^2(W_{XX} + W_{YY}) + W_{ZZ}] \tag{14c}$$

$$0 = U_X + V_Y + W_Z \tag{14d}$$

where Eqs. (14a–14d) apply for both fluids. The subscripts in the above equations represent derivatives with respect to the scaled variable. The boundary conditions at the upper and lower surface are not changed by the scaling.

The focus of this study is confined films where a viscosity ratio of the film to bounding fluid is large $(\mu_1/\mu_2 \gg 1)$. Therefore, in the fluid films studied, the bounding fluid acts like an inert gas and eliminates the requirement for solving the evolution equations for both fluids. Since the fluid film is thin ($h_0 < 100$ nm), the inertial effects will be negligible ($\mathrm{Re} = \rho u_0 h_0/\mu \ll 1$). These simplifications, along with consideration of the leading order terms in Eqs. (14a–14d), yield:

$$-(P_X + \Phi_X) + U_{ZZ} = 0 \tag{15a}$$

$$-(P_Y + \Phi_Y) + V_{ZZ} = 0 \tag{15b}$$

$$P_Z + \Phi_Z = 0 \tag{15c}$$

$$U_X + V_Y + W_Z = 0 \tag{15d}$$

The fluid properties are assumed constant in space and time in the derivation of Eqs. (15a–15d). Equations (15) form the basis for the derivation of the interface motion equation. The boundary conditions used are:

$$\vec{U} = 0 \quad \text{at } z = 0 \tag{16a}$$

$$U_Z = V_Z = 0 \quad \text{at } z = h(x, y, t) \tag{16b}$$

$$P - P_{\mathrm{ext}} = \gamma(H_{XX} + H_{YY}) \quad \text{at } z = h(x, y, t) \tag{16c}$$

where P_{ext} is the external reference pressure (set to zero). The kinematic condition at the fluid interface $z = h(x, y, t)$ is also used to relate the temporal changes of the interface to the fluid velocity:

$$H_T + UH_X + VH_Y = W \tag{17}$$

The interface motion equation is derived using the system of equations shown in (15) with the boundary conditions from (16) and the kinematic condition (17).

Extracting the relationships between the scaled velocity components U, V, and W with the scaled film thickness, H, and the pressure, P, from the above equations leads to the final evolution equation for the film:

$$\frac{\partial H}{\partial t} + \frac{\partial}{\partial X}\left[H^3\frac{\partial \Psi}{\partial X}\right] + \frac{\partial}{\partial Y}\left[H^3\frac{\partial \Psi}{\partial Y}\right] = 0 \tag{18}$$

where

$$\Psi = \frac{\partial^2 H}{\partial X^2} + \frac{\partial^2 H}{\partial Y^2} - \Phi \tag{19}$$

The function Φ represents the overall body forces acting on the film, which results from intermolecular and electrostatic interactions.

The intermolecular forces considered in the present work consists of a long range Lifshitz-van der Waals (LVDW) force and a short ranged repulsion similar to Born repulsion. The energy per unit volume or conjoining/disjoining pressure in the film due to the LVDW forces can be written as[2, 13]

$$\phi_{\mathrm{LVDW}} = \frac{A_L}{6\pi h^3} \tag{20}$$

RESEARCH ARTICLE

where A_L is the effective Hamaker constant for interactions between the upper (free) surface of the film and lower solid through the fluid film. The above expression diverges when the film dries out at the lower solid substrate ($h = 0$). This divergence is prevented by considering a repulsive force that maintains a minimum equilibrium liquid thickness on the substrate as suggested by Mitlin.[14] In this work, an absorbed layer of thickness $l_0 = 1$ nm is maintained on either solid surface. A 1 nm thick absorbed layer does not significantly influence the film drainage while ensuring the continuity assumption remains valid. The close range repulsive term takes the form:

$$\phi_{BL} = -\frac{8B_L}{h^9} \tag{21}$$

The close range repulsive constant, B_L, is found by setting the conjoining/disjoining pressure equal to zero at the lower surface ($\phi(z = l_0) = 0$).

The electrostatics driven drainage of the film is caused by the Maxwell stress at the fluid interface. This stress is computed by solving for the electric potential distribution between the two electrodes represented by the Laplace equation

$$\nabla^2 \psi_i = 0 \quad (i = 1, 2) \tag{22}$$

where ψ_i is the potential in fluid $i = 1, 2$. The boundary conditions for the electrostatic problem are defined as

$$\begin{aligned} &\psi_1 = \psi_{\text{low}} && \text{at } z = 0 \\ &\psi_1 = \psi_2 && \text{at } z = h(x, y, t) \\ &\epsilon_1 \frac{\partial \psi_1}{\partial z} = \epsilon_2 \frac{\partial \psi_2}{\partial z} && \text{at } z = h(x, y, t) \\ &\psi_2 = 0 && \text{at } z = d \end{aligned} \tag{23}$$

The above system of equations can be solved analytically for a thin film trapped between two homogeneous electrodes. The potential energy per unit area due to the electrostatic interaction and the electric field at the film-bounding fluid interface, respectively, are given by:[4]

$$\phi_{\text{EL}} = -0.5\epsilon_0\epsilon_p(\epsilon_p - 1)E_p^2 \tag{24}$$

and

$$E_p = \frac{\psi_{\text{low}}}{\epsilon_p d - (\epsilon_p - 1)h} \tag{25}$$

Here, $\epsilon_p = \epsilon_1/\epsilon_2$ is the ratio of relative permittivity of the film liquid to the bounding fluid.

The contributions of electrostatics and the intermolecular body forces are added to yield the total conjoining/disjoining pressure

$$\phi = \phi_{\text{LV DW}} + \phi_{\text{BL}} + \phi_{\text{EL}} \tag{26}$$

2.2. Scaling

The problem scaling is derived from a linear stability formulation for the thin film equation. The general form for the time (t^*) and length (x^*) scales as given by Verma et al.[13] from the linear stability analysis are

$$t^* = \frac{12\mu\gamma}{h^3(\partial\phi/\partial h)^2} \quad x^* = \sqrt{\frac{-8\pi^2\gamma}{\partial\phi/\partial h}} \tag{27}$$

In the case of pressure dominated flow, where only LVDW forces are present, the time and length scales can be found using Eq. (27). Following the work of Khanna and Sharma,[12] the time (t^*) and length (x^*) scaling, as well as the dominant length scale (λ_c), for a pressure dominated flow are

$$t^* = \frac{12\pi^2\mu\gamma h_0^5}{A_L^2} \quad x^* = h_0^2\sqrt{\frac{2\pi\gamma}{A_L}} \tag{28}$$

$$(\lambda_c)_{\text{LV DW}} = 2\pi h_0^2\sqrt{\frac{2\pi\gamma}{A_L}} \tag{29}$$

The scaling for an electrostatically dominated flow is

$$\begin{aligned} t^* &= \frac{3\mu\gamma h_0^3}{[0.5\epsilon_0\epsilon_p(\epsilon_p - 1)\psi_{\text{low}}^2]^2} \\ x^* &= 2\pi\sqrt{\frac{\gamma h_0^3}{0.5\epsilon_0\epsilon_p(\epsilon_p - 1)\psi_{\text{low}}^2}} \end{aligned} \tag{30}$$

$$(\lambda_c)_{\text{EL}} = 2\pi\sqrt{\frac{2\gamma\psi_b}{\epsilon_0\epsilon_p(\epsilon_p - 1)^2}}E_p^{-3/2} \tag{31}$$

3. NUMERICAL METHOD

The solution methodology employed was the discretization of spatial derivatives using finite differences to reduce the partial differential equation system to a differential-algebraic equation (DAE) system in time, which was then solved employing a differential algebraic solver (DASSL).[15] In the simulations performed, a uniform cartesian grid was used. The thin film evolution equation was discretized using central differences in a pseudo staggered grid approach. The simulations were performed on a film cross-section of dimensions 7.77 μm $\times$ 7.77 μm and grid size used to discretize the spatial domain (X, Y) was 60×60. The time steps were modified adaptively by the DAE solver.

The discretization scheme was formulated to avoid so-called 'checker boarding' in the solution. This formulation requires mid-point values for the film thickness, which are used in the non-linear terms. The mid-point values can either be approximated based on calculated values or obtained by solving additional equations. The latter would require an additional set of $(n_x - 1)(n_y - 1)$ equations and

the storage of accompanying values. Since significantly increasing the number of equations was not desirable, the mid-point values were approximated using a third order Everett's method.[16]

In the problems considered in this work, periodic boundary conditions were employed. In this case, the assumption was that the portion of the domain modeled was repeated as periodic images over the entire system. This means that any flow out of a boundary will result in inflow on the opposite boundary. Following,[11] the boundary condition implies that the first and last points on a row or column of mesh are equal. This means that a continuity of derivatives occurs over the boundaries.

The initial condition for the problem was assigned as a random small-amplitude perturbation of the height, H, around the initial equilibrium film thickness ($H_0 = h/h_0 = 1$). The maximum amplitude of the perturbation was *ca.* 1% of the initial scaled height.

A fortran program was developed to implement the solution algorithm. The program was run on a personal computer with an Intel Pentium IV 2 GHz processor and 2 GB RAM. A typical dynamic simulation required about two hours of run time for completion.

4. RESULTS AND DISCUSSION

In this section, we compare the evolved film morphologies and the time scales observed during pressure based and electrostatically driven drainage of thin films. The comparison of film morphologies pertain to qualitative observations of the film structures and length scales of dominant features. The comparison of time scales is conducted by studying the times required to attain the final pseudo-stationary states starting from the initial uniform thickness. All simulations were performed for a homogeneous liquid film formed on a chemically homogeneous substrate.

4.1. Pressure Based Drainage

Here, we examine pressure based drainage on a homogeneous substrate. In pressure based drainage, only LVDW interactions influence the film drainage. The base line parameters for pressure induced drainage on a homogeneous substrate are shown in Table (I). The values in Table (I) were used for all simulations that follow, unless explicitly stated otherwise.

Figure 2 shows the time evolution of the pressure based drainage for an initially 20 nm thick film. A square domain of side $L = 2\lambda_c$, where λ_c is given by Eq. (29), was used in these simulations. The domain was discretized into a 60×60 cartesian grid. The gray-scale levels represent the non-dimensional film thickness. The film drains from a small initial random perturbation, eventually forming a coherent structure of depressions and bumps. Some of the depressions randomly turn into the fastest draining parts of the film and eventually completely drain to form circular holes. The number of holes then grows, and in the final stages of the drainage, the spacing between two adjacent holes (shown in the final image of Fig. 2) is $1.38\lambda_c$. Linear theory predicts that hole spacing in pressure based drainage should have a spacing of $\sqrt{2}\lambda_c$. Thus, our numerical simulations seem to be in reasonable agreement with linear theory.[12]

Table I. Base line parameters employed in the simulations for thin film drainage.

Parameter	Value
Viscosity (film, μ)	1 Pa s
Interfacial tension (γ)	0.038 N/m
Relative permittivity ratio (ϵ_p)	2.5 [−]
Electrode spacing (d)	100 nm
Initial film thickness (h_0)	20 nm
Film dimension (square) (L)	7.77 μm
Effective Hamaker constant (A_L)	1×10^{-19} J
Short-range repulsion constant (B_L)	6.63×10^{-76} J/m^6

The time evolution of the non-dimensional film thickness along a section shown by the dashed line in Figure 2(f) is depicted in Figure 3. The $2D$ section views show the non-dimensional film thickness corresponding to the slice at $Y = 5.0256$. The section cut was chosen so that it intersected the first hole that forms in the domain. The figure shows that ridges or lips form around the edges of the hole. It also demonstrates the film's behavior away from the hole. As holes or dry spots in the film form, the remainder of the film thickens and assumes a new equilibrium height but is otherwise not influenced by the formation of the hole. Pressure driven film drainage results

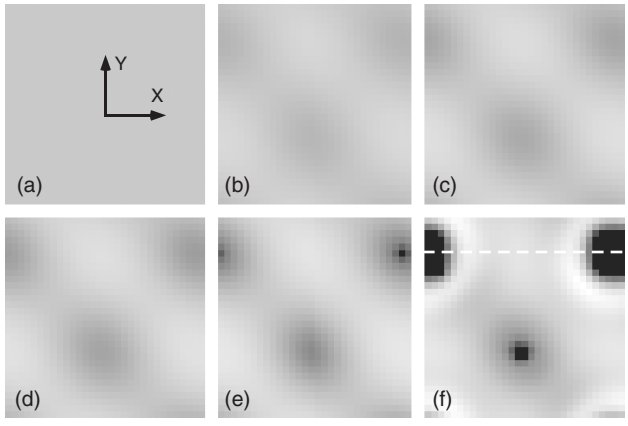

Fig. 2. Evolution of a 20 nm thick film taken as gray scale images of the film thickness. The times corresponding to the snapshots are (a): 0.58, (b): 21.40, (c): 30.82, (d): 32.98, (e): 35.14, and (f): 35.72 seconds. A six level linear gray scale was used in all images shown. The maximum is 25.96 nm (white) and the minimum is 1 nm (black). All other parameters were taken as base line values (Table (I)). The mean thickness of the film in (a) is 20 nm, with a $<1\%$ amplitude random perturbation. The scaled dimensions in the X and Y directions in each panel range from -2π to 2π. The origin is located at the center of each panel (shown in panel (a)).

RESEARCH ARTICLE

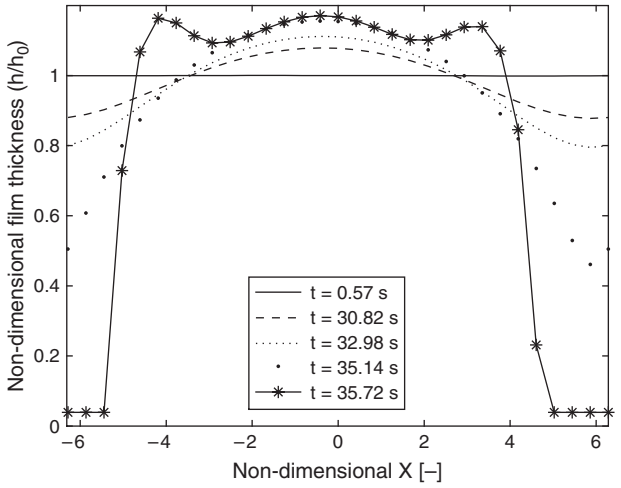

Fig. 3. Section views of the non-dimensional film thickness at different times. The section views are taken at $Y = 5.0256$ (dashed line in panel (f) of Fig. 2). All other parameters were taken as base line values (Table I).

in the formation a series of circular holes and surrounding ridges. The drainage is very slow at the initial stages, while the final morphology is attained very rapidly over the last few seconds.

4.2. Electrostatic Drainage

Figure 4 shows a series of gray scale images that represent the final film structures formed by drainage of an initially 20 nm thick film subjected to increasing initial applied electric fields, *cf.* Eq. (25), on a uniform domain size of $L = 7.77$ μm. As the magnitude of the applied electric field is increased, the maximum height that the film attains increases. Comparing panels (a) and (b) of Figure 4, it is apparent that the final film morphology observed for solely pressure based drainage ($E = 0$, panel (a)) is quite similar to the structure observed in presence of an applied electric field of 0.45 MV/m (panel (b)). When the applied field is increased another order of magnitude to 4.50 MV/m (panel (c)), the film morphology changes noticeably. The hole growth becomes more uniform, with the size of the holes that form becoming almost equal. The application of small electric fields, even as low as 4.50 MV/m add uniformity to the structure that is formed. This behavior is also observed in panel (d) corresponding to an applied field of 11.36 MV/m. When the applied field was increased to 27.27 MV/m (panel (e)), the film morphology again changes significantly. The size of the holes that form is reduced and localized elevated patches or columns can be seen. As the magnitude of the applied field is increased to 45.45 MV/m (panel (f)), the size of holes and columns that form becomes even smaller.

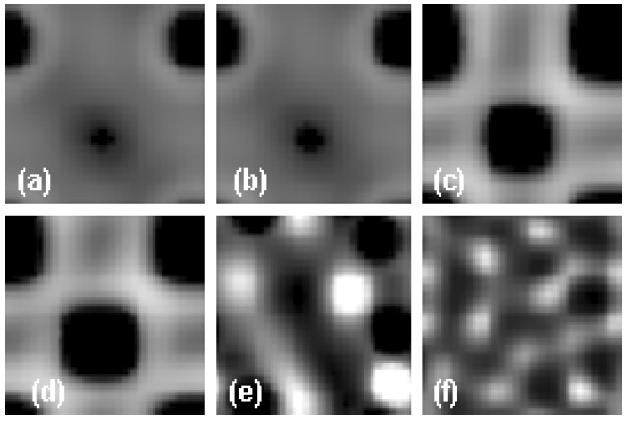

Fig. 4. Comparison of final film structures for a 20 nm film subjected to different magnitudes of electric field. The magnitude of the initially applied electric fields at the interface are (from panel a to panel (f), respectively): $E_p = 0$, 0.45, 4.50, 11.36, 27.27, and 45.45 MV/m. A linear gray scale is shown in all images with a maximum value of 39.61 nm (white) to a minimum value of 1 nm (black). All other parameters are as stated in Table I.

The morphology of the drained film clearly indicates how increase in the applied field above a threshold value of *ca.* 5 MV/m changes the nature of drainage. At higher applied fields, the film morphology develops subtle differences from those obtained under solely pressure driven drainage. With the application of an electric field of magnitude > 25 MV/m, the film drainage becomes dominated by electrostatic effects, as evidenced by formation of columnar structures separating smaller holes, as well as an increase in the density of features observed over the simulated region. The application of an electric field will also increase the maximum observed film thickness, and in the case where large fields are applied ($E_p > 25$ MV/m) columns will form.

Figure 5 shows the evolution of the minimum non-dimensional film thickness with time. The minimum

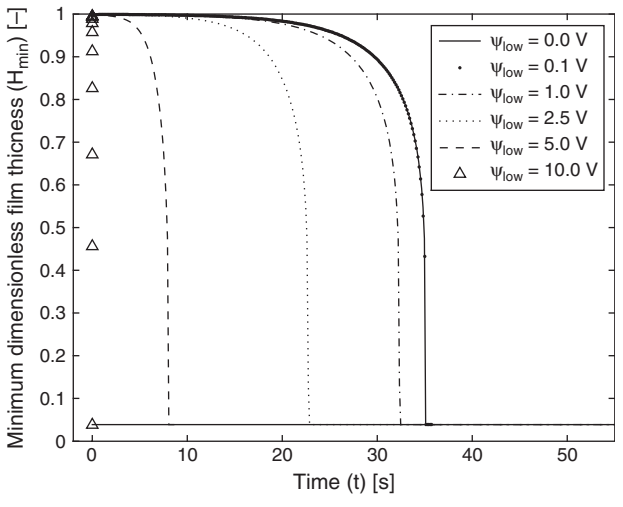

Fig. 5. Minimum non-dimensional film thickness for an initially 20 nm thick film for various applied potentials on the lower electrode, ψ_{low}, keeping the upper electrode grounded. The initial electric fields at the interface (E_p) corresponding to these potentials are shown in Figures 4(a)–(f), respectively. The minimum thickness corresponds to the fastest draining location on the film. All other parameters are as stated in Table I.

thickness was found by locating the fastest growing hole and tracking its drainage. The drainage time decreases as the magnitude of the applied voltage on the lower electrode, ψ_{low}, and therefore, the initial electric field at the interface, *cf.* Eq. (25), is increased. Note that the electric field changes with time as the film morphology evolves in each simulation, although the applied potential, ψ_{low} remains fixed. For applied voltages of up to 0.1 V, no perceptible change in the drainage behavior compared to pressure based drainage is observed. At higher applied potentials, the drainage becomes quicker. The initial decrease in height is almost independent of the applied potential, following which, a rapid change in height with time is observed. As the magnitude of the applied electric field is increased, the time taken to attain the final height is considerably reduced. Finally, at applied voltage of 10 V, the drainage is virtually instantaneous compared to the time taken for drainage of a film under the influence of purely van der Waals interactions.

5. CONCLUDING REMARKS

Numerical simulations of thin film drainage employing the long wave approximation were conducted to compare the drainage behavior under influence of pressure and an applied electric field across the film. It is noted that apart from morphological differences in the final film structures obtained under these conditions, there is also a significant difference in time scales of the drainage, with electrostatic drainage becoming almost instantaneous compared to pressure based drainage at high applied fields. These observations indicate that drainage of films by application of electric field follows considerably different dynamics compared to pressure based drainage.

Acknowledgment: Financial support from NSERC is gratefully acknowledged.

References

1. A. Oron, S. H. Davis, and S. G. Bankoff, *Rev. Mod. Phys.* 69, 931 **(1997)**.
2. Ruckenstein and R. K. Jain, *J. Chem. Soc. Faraday Trans. II* 70, 132 **(1974)**.
3. A. Sharma and A. T. Jameel, *J. Colloid Interface Sci.* 161, 190 **(1993)**.
4. R. Verma, A. Sharma, K. Kargupta, and J. Bhaumik, *Langmuir* 21, 3710 **(2005)**.
5. E. Schaffer, T. Thurn-Albrecht, T. P. Russell, and U. Steiner, *Nature* 403, 874 **(2000)**.
6. L. F. Pease and W. B. Russel, *J. Non-Newtonian Fluid Mech.* 102, 233 **(2002)**.
7. V. Shankar and A. Sharma, *J. Colloid Interface Sci.* 274, 294 **(2004)**.
8. N. Wu, L. F. Pease, and W. B. Russel, *Langmuir* 21, 12290 **(2005)**.
9. N. Wu, L. F. Pease, and W. B. Russel, *Adv. Funct. Mat.* 16, 1992 **(2006)**.
10. F. Mostowfi, K. Khristov, J. Czarnecki, J. Masliyah, and S. Bhattacharjee, *Appl. Phys. Lett.* 90, 184102 **(2007)**.
11. M. B. Williams and S. H. Davis, *J. Colloid Interface Sci.* 90, 220 **(1982)**.
12. R. Khanna and A. Sharma, *J. Colloid Interface Sci.* 195, 42 **(1997)**.
13. R. Verma, A. Sharma, I. Banerjee, and K. Kargupta, *J. Colloid Interface Sci.* 296, 220 **(2006)**.
14. V. S. Mitlin, *J. Colloid Interface Sci.* 156, 491 **(1993)**.
15. R. S. Maier, L. R. Petzold, and W. Rath, *Proc. Scalable Parallel Libraries Conference* **(1993)**, pp. 174–182.
16. F. S. Acton, Numerical Methods that Work, Harper and Row **(1970)**.

Received: xx October 2007. Accepted: xx December 2007.

RESEARCH ARTICLE